Preparation and probing of coherent vibrational wave packets in the ground electronic state of HD^+

Rangana Bhattacharya,* Souvik Chatterjee, and S. S. Bhattacharyya

Atomic and Molecular Physics Section, Department of Materials Science, Indian Association for the Cultivation of Science, Jadavpur, Kolkata 700 032, India

(Received 12 December 2011; published 27 March 2012)

We have investigated the formation of coherent vibrational wave packets in the ground electronic state of HD^+ on exposure to intense ultrashort laser pulses of wavelength 1060 nm. The effects of the duration and field strength of the pulse on the final composition of the residual bound nuclear wave packet generated by such impulsive excitations have been studied. The resulting wave packet is allowed to evolve freely on the potential surface for some time, after which a weak pulse of sufficiently large duration is used for probing its composition. This pulse can cause only single-photon dissociation. The simulations have been performed with different probe wavelengths for accessing information about different portions of the wave packet in the vibrational quantum number space. Our aim was to investigate the extent to which information obtained from the kinetic-energy spectra of the photofragments induced by the probe pulse can be correlated to the structure of the wave packet. Simple time-dependent perturbation calculations have also been performed for obtaining the relative strengths of photofragment signals arising from different vibrational levels due to wave-packet dissociation. A comparison with our numerical results indicates that though the general features of the photofragment kinetic-energy spectra from a wave packet are consistent with the perturbation theory results in the intensity regime studied, dynamical evolution during a long pulse can modify the relative heights of the kinetic-energy peaks through nonperturbative interactions in some cases.

DOI: 10.1103/PhysRevA.85.033424 PACS number(s): 33.80.Wz, 42.50.Hz, 33.80.Gj

I. INTRODUCTION

When an atomic or molecular system in a stationary state is exposed to an intense electromagnetic radiation field, its wave function becomes nonstationary, being a superposition of many eigenstates. Thus an ultrashort IR pulse acting on a molecule in a stationary state can be thought of as providing an impulsive excitation creating a wave packet. The constitution of the wave packet in terms of the stationary states will depend on the nature of the impulse, which can be parametrized by its time duration, temporal shape, peak intensity, and the central frequency. After the pulse, this nonstationary wave packet continues to evolve in time without changing its constitution. Information about the nature and time evolution of such wave packets can be obtained theoretically from the solution of the time-dependent Schrödinger equation. In the laboratory this problem of studying the wave packet is generally tackled by introducing another pulse, called a probe pulse, applied after a certain time delay. The characteristics of such a probe pulse will depend upon the objective, i.e., the information one wishes to obtain. The probe pulse can be designed to cause ionization or dissociation from the wave packet and the study of such ionization or dissociation signals can provide important information about the wave-packet dynamics, enriching our understanding of molecular processes. Such interaction of fields with wave packets may also provide opportunities for their manipulation which can be extended to interesting applications such as control of reaction dynamics of important chemical or biological systems as well as use of such control techniques in the field of quantum information.

Zewail and co-workers were one of the pioneering groups adopting the technique of wave-packet generation by exciting molecules with a femtosecond laser pulse and then monitoring the time evolution of the wave packet with a time-delayed probe pulse [1,2]. Their ultimate goal was the direct viewing of nuclear motion, through knowledge of the time evolution of the wave packet. Accurate information about the time evolution of the nuclear wave function is of great interest in chemical dynamics. A conceptually simple method of observing the dimension and motion of the nuclear wave packets is to induce Coulomb explosion by a delayed femtosecond laser [3]. The possibility of imaging the initial nuclear probability distribution from the fragment kinetic-energy spectra of protons in the case of H_2^+, through such an optical Coulomb explosion, was reported in Refs. [4–6] (using both UV as well as IR intense ultrashort laser pulses). The availability of intense few-cycle laser pulses have significantly advanced the pump-probe techniques designed in the early 1990s for real-time observation of ultrafast atomic and molecular processes, as evidenced in Refs. [7–9]. It has been demonstrated in Ref. [7] that dissociating as well as bound wave-packet motion can be visualized by the use of intense ultrashort pump-probe laser systems. Another example is provided by the simultaneous mapping of the evolving wave-packet components on two different potential surfaces in cases of H_2^+ and D_2^+ [8]. It was shown in [9] that the dynamics of diatomics and triatomics can be imaged in a manner demonstrated in the previous examples. A combination of the pump-probe method and the Coulomb explosion imaging technique can allow high-resolution real-time mapping of nuclear wave packets, as demonstrated in a series of works [10–17]. The application of femtosecond pump-probe experiments for generation of coherent nuclear wave packets and its time-resolved imaging are discussed in detail by Calvert *et al.* in a recent report [17]. In Ref. [18]

*Present address: Experimental Condensed Matter Physics Division, Saha Institute of Nuclear Physics, Sector-1, Block-AF, Bidhannagar, Kolkata 700064, India.

ab initio calculations for tracing of vibrational wave packets in the excited electronic state created by nondissociative single ionization of H_2 through a pump-probe scheme, have been reported.

The imaging of wave-packet dynamics is also possible by molecular fragmentation induced by a time-delayed probe pulse. In Refs. [19–21] the molecular system is probed via the photodissociation channel through bond softening or above-threshold dissociation. However in Ref. [20] wave-packet evolution is observed by an additional route of double ionization.

Imaging wave packets has also made possible the visualization of certain purely quantum-mechanical phenomena such as interference between two dissociating nuclear wave packets [22], as well as the manipulation of vibrational wave-packet interferences for a single molecule [23]. Katsuki *et al.* have succeeded in measuring pronounced interference structures developed due to the overlap of two counterpropagating wave packets on an excited electronic state in iodine molecule by using probe lasers with wavelengths in the range 382–391 nm [24].

A somewhat different mechanism of generation of a ground-state vibrational wave packet was investigated by Goll *et al.* [25]. In their work a vibrational wave packet of H_2 in its electronic ground state was formed through the strong dependence of the tunnel ionization rate of this molecule (by a pump pulse) on the internuclear H-H separation. They also simulated the probing of the vibrational wave packet. In the probing the wave-packet motion is well reflected in the oscillatory behavior of ionization yield as a function of the delay time between the pump and the probe pulse. The theoretical prediction was also experimentally confirmed in Ref. [26], in which observation of ground-state vibrational wave packets for a D_2 molecule was reported.

The bound and dissociating nuclear wave-packet motion can be mapped using different detection methods. Some of the other methods for detection of laser-induced ultrafast processes are fluorescence detection of pump-probe signals, ion detection, photoelectron spectroscopy, time-resolved electron diffraction, etc. and these have been reviewed in Ref. [27].

In recent times different techniques of dynamic imaging of nuclear wave packets with angstrom-level spatial resolution and subfemtosecond time resolution have been developed. An extensive topical review of such imaging techniques has been given by Altucci *et al.* [28]. The imaging techniques using ultrashort laser pulse mostly depend on the release of electronic wave packets and their recollision with the residual ion within a single optical cycle. Since the released electronic wave packet remains entangled with the bound electronic wave function, various processes occurring during recollision can be used as tools for exploration of nuclear dynamics with subfemtosecond resolution. In such processes a single laser pulse is involved and the molecule can be said to provide its own probe in the form of correlated electronic wave packets. The processes include harmonic generation, double ionization, Coulomb explosion, and fragmentation of the residual molecular ion. A discussion of methods based on such phenomena can be found in Ref. [29]. Examples of attosecond probing of vibrational dynamics with high-harmonic generation can be found in the works of Lein [30] and Baker *et al.* [31]. A very recent review of this field can be found in Ref. [32]. Kinetic-energy analysis of fragments of molecular ions arising from inelastic scattering of the electron has been used as a probe in Ref. [33].

Thus obtaining temporally highly resolved information about the spatial structure of nuclear wave packets would require the use of extremely short pulses and self-probing methods. Such pulses, because of their very broad energy spectrum, probe the wave packet simultaneously over a large region of energy space. However, if we are interested in the composition of nuclear wave packets in terms of vibrational states, or in other words, if we want information about the wave packet in the vibrational quantum number space, we should use sufficiently weak and long pulses which will probe the wave packet over a large region of configuration space. In some sense the information obtained will be complementary to that using self-probe.

In the present work, we subject the heteronuclear polar molecular ion HD^+ to an intense ultrashort IR laser pulse of duration of a few femtoseconds, and study how the duration and intensity of the pulses determine the composition of the residual wave packet remaining bound in the ground electronic state of HD^+. These nonstationary wave packets, obtained from impulsive excitation of different stationary vibrational states, are allowed to freely evolve on the potential surface. A comparatively weak pulse of sufficiently long duration, which causes dissociation from the wave packet, is introduced for the purpose of probing. Different frequencies of the probe pulse can provide information about different portions of the wave packet in the vibrational quantum number space. Our aim is to see how the information from the kinetic-energy spectra of the photodissociation fragments for various probe pulses can be correlated to the constitution of the wave packet. In fact, in some recent works it has been demonstrated that the examination of the kinetic-energy spectra obtained after ionization or dissociation from a wave packet can be used for the identification of the constituting vibrational state components in the nuclear wave packet. In Ref. [34] the experimentally observed kinetic-energy spectrum was well correlated to the theoretically calculated relative population in the different vibrational levels in H_2^+. Very recently experimental observation of vibrationally resolved structures in O_2^+ due to dissociation induced by intense ultrashort laser pulses have been reported in Ref. [35]. In another theoretical work [36] the proton energy distribution generated by an IR laser pulse was used for the identification of the vibrational composition of the nuclear wave packet, which was generated by a single attosecond pulse or a train of attosecond pulses. Use of different intensities as well as pulse durations for probing allows us to investigate the nature of changes in the vibrational wave packet due to the probe pulses themselves. In the present work we investigate how the generation of coherent vibrational wave packets by ultrashort laser pulses as well as their weak-field probing can help in the better understanding of molecular dynamics.

II. THEORY

The study of wave-packet generation by impulsive excitation and probing of the generated wave packets with laser pulses in the case of HD^+ molecular ions essentially involves the solution of the time-dependent Schrödinger equation

for the nuclear motion in the presence of two consecutive time-delayed linearly polarized laser pulses. This solution is made in the basis of the two lowest electronic states of HD^+. These two states are obtained from the Born-Oppenheimer molecular states $1s\sigma_g$ and $2p\sigma_u$, by including the nonadiabatic g-u symmetry-breaking coupling term between them, arising from mass asymmetry of the heteronuclear ion, in the full Hamiltonian. This removes the degeneracy between the two molecular orbitals in the large internuclear separation limit and causes the asymptotic energies of the two electronic states to converge to their proper atomic orbital energy values. Henceforth we denote the modified (rediagonalized) ground- and first excited electronic states obtained in this way as GS and ES, respectively. At each internuclear separation R, we can write the nuclear wave functions Ψ_G and Ψ_E in this proper basis (in which the molecular orbitals asymptotically go to the correct atomic limit), as linear combinations of the nuclear wave functions Φ_g and Φ_u in the Born-Oppenheimer basis [37–39].

$$\Psi_G(R,t) = a(R)\Phi_g(R,t) + b(R)\Phi_u(R,t), \tag{1}$$

$$\Psi_E(R,t) = -b(R)\Phi_g(R,t) + a(R)\Phi_u(R,t), \tag{2}$$

where $a(R)$ and $b(R)$ represent the coupling coefficients satisfying the unitarity relation $a^2(R + b^2(R) = 1$. These mixing coefficients a and b, along with the potential energies $V_G(R)$ and $V_E(R)$ of the two new electronic states GS and ES, calculated earlier [40,41], have been used by us. How the R dependences of the mixing coefficients induce the nonadiabatic coupling between the two components of the nuclear wave packet has been discussed in detail in Ref. [39].

The states of nuclear motion Ψ_G and Ψ_E on each of these two electronic states GS and ES are subdivided into groups of different parities, even (e) and odd (o) [37–39], for taking into consideration all possible, permanent dipole-moment-induced intraelectronic radiative couplings. This essentially involves a four-component wave packet for the two electronic states for which the Schrödinger equation becomes

$$i\hbar\frac{\partial}{\partial t}\begin{pmatrix}\Psi_{G_e}(R,t)\\ \Psi_{G_o}(R,t)\\ \Psi_{E_e}(R,t)\\ \Psi_{E_o}(R,t)\end{pmatrix} = H(R,t)\begin{pmatrix}\Psi_{G_e}(R,t)\\ \Psi_{G_o}(R,t)\\ \Psi_{E_e}(R,t)\\ \Psi_{E_o}(R,t)\end{pmatrix}, \tag{3}$$

with

$$H = -\frac{\hbar^2}{2m}\frac{\partial^2}{\partial R^2} + V(R,t). \tag{4}$$

Here, m is the reduced mass of the nuclei and R is the internuclear separation. $V(R,t)$ is the potential matrix, in the four-component basis, including both the diagonal internuclear potentials and the off-diagonal interstate as well as intrastate radiative couplings resulting from the external electromagnetic fields. The solution of the time-dependent Schrödinger equation essentially starts with an initial wave packet as the vibrational eigenfunction of arbitrarily defined parity. The potential matrix can be written as

$$V(R,t) = \begin{pmatrix} V_G(R) & -\mu_{GG}(R)E(t) & 0 & -\mu_{EG}(R)E(t)\\ -\mu_{GG}(R)E(t) & V_G(R) & -\mu_{EG}(R)E(t) & 0\\ 0 & -\mu_{EG}(R)E(t) & V_E(R) & -\mu_{EE}(R)E(t)\\ -\mu_{EG}(R)E(t) & 0 & -\mu_{EE}(R)E(t) & V_E(R)\end{pmatrix}. \tag{5}$$

We first calculate the time evolution of the initial wave packet due to the intense, ultrashort pump pulse. Once the pulse is over, we allow time evolution of the resulting wave packet on the field-free potential surfaces for some time. During this time any eventually dissociating part of the wave packet leaves the region of interaction and will not further interact with the probe pulse. Only the residual bound portion of the wave packet will remain.

The pump and probe fields used for the numerical simulation are both sine-squared-shaped pulses, so that the electric field is

$$E(t) = \sum_{i=1}^{2} E_i^0 f_i(t)\cos(\omega_i t), \tag{6}$$

where

$$f_i(t) = \sin^2\left\{\frac{\pi(t-\tau_i)}{2\sigma_i}\right\}, \quad \text{for} \quad 0 < (t-\tau_i) < 2\sigma_i \tag{7}$$

and 0 otherwise. $i = 1$ and 2 for the pump and probe pulse, respectively, and $\tau_1 = 0$ and τ_2 is the delay time between the two pulses. $E_{1,2}^0$ are the peak magnitudes of the electric field of the two pulses and $2\sigma_{1,2}$ are the respective total pulse durations.

$\mu_{G-G}(R)$ and $\mu_{E-E}(R)$ are the R-dependent permanent dipole moments in the two electronic states and $\mu_{G-E}(R)$ is the R-dependent transition dipole moment. The expression for the transition and permanent dipole matrix elements between the asymptotically correct states in terms of the transition moment between the two lowest Born-Oppenheimer states are shown in Ref. [38].

The split operator Fourier transform method is employed for the computation of the action of the time evolution operator $e^{-i[(H/\hbar)\delta t]}$on the wave packet at each instant of time. The expression for the time evolution operator involves the exponential of the sum of the noncommutating kinetic and potential operators. For the time propagation from time t_{n-1} to t_n ($t_{n+1} - t_n = \delta t$, this operator is approximated as

$$\begin{aligned} U(t_{n+1} \leftarrow t_n) &= e^{-i[(H/\hbar)\delta t]}\\ &= e^{i[(\hbar/2\mu)(\partial^2/\partial R^2)(\delta t/2)]}e^{-i[V(R,t_n)\delta t/\hbar]}\\ &\quad\times e^{i[(\hbar/2\mu)(\partial^2/\partial R^2)(\delta t/2)]}. \end{aligned} \tag{8}$$

This expression is correct to second order in δt.

During the wave-packet propagation the part of the operator involving the kinetic energy has a diagonal representation in the momentum space, and so is made to act on the momentum space wave functions obtained from Fourier transform of the coordinate space wave functions in the Born-Oppenheimer basis. The part involving the potential energy operator must operate on the coordinate space wave functions in the G-E basis, since the dipole moments are expressed in this basis. At each time step fast Fourier transform (FFT) allows the wave-packet components to switch between the coordinate space and momentum space representations.

In order to calculate the kinetic-energy spectrum of the photofragments we use the artifact of dividing the coordinate space for the wave-packet propagation, into two regions, the interaction and the asymptotic region. The wave-packet components at any instant may be written as the sum of the wave functions in these two regions $\Psi(R,t) = \Psi_I(R,t) + \Psi_A(R,t)$. At every time step a small portion from each wave-packet component may cross over the boundary from the interaction region to the asymptotic region and all these components are added to the momentum representation of $\Psi_A(R,t)$ to obtain the final outgoing asymptotic wave function in this representation. The boundary between the two regions is chosen as 40 a.u. The wave-packet propagation is continued up to 50 000 a.u. of time ($\sim$1.2 ps), long after the radiation field is switched off, so that all the portions of the dissociated wave-packet components get sufficient time to reach the asymptotic region, thereby giving a stable kinetic-energy distribution.

The vibrational distribution of the residual population in the ground electronic state after the pump pulse is obtained by projection of the final nuclear wave-packet component of the GS state in the interaction region, at a time t, on the different field-free vibrational levels.

$$\langle \Psi_v(R) \mid \Psi_{(G)}(R,t) \rangle_R. \tag{9}$$

The time t must be taken sufficiently large so that all eventually dissociating portions of the ground-state wave packet can escape the interaction region.

In the present work we have also invoked the perturbation theory expressions for the transition probabilities into the continuum from various vibrational levels and have compared them with the pattern of peak heights in the kinetic-energy spectra obtained due to dissociation induced by the probe pulse. The transition probabilities for the three different probe frequencies obtained from the Fermi golden rule have been multiplied by the initial populations of the different vibrational eigenstates constituting the wave packet.

III. RESULTS AND DISCUSSIONS

The formation of coherent vibrational wave packets under impulsive excitation by short femtosecond pump laser pulses, starting from different stationary eigenstates in the ground electronic state of HD^+, has been explored. The usual two electronic states approximation has been adopted. Thus photodissociation is the only loss process considered in our theoretical investigations. A $\sin^2$-shaped laser pulse with a carrier wavelength of 1060 nm and of very short duration, 2σ (2σ = 5, 10, or 15 fs) creates the vibrational wave packet. Different peak intensities of this pulse have been used. Three different vibrational levels, v = 0, 2, and 4 were chosen as initial states. Our motivation is to investigate the final composition of the coherent wave packets prepared by such intense ultrashort pulsed laser fields. We also investigate the dynamics of such coherently excited wave packets under comparatively weak and long probe pulses of various frequencies, pulse times, and intensities within the same two-state framework. In this part of the work the main motivation is to analyze the kind of information that can be obtained from the kinetic-energy spectra of the photofragments arising from the dissociative decay of the wave packets.

The parameters of the pump pulse (specified by its peak intensity, duration, pulse shape, and the polarization), which prepares the wave packet on the ground electronic state are expected to play significant roles in determining its overall composition and motion. Recent experiments have employed ultrashort pump pulses of duration 4–15 fs and intensity in the range 5 to 8 $\times$ 10^{14} W/cm^2, to initiate vibrational wave-packet dynamics [8–16,19,20]. Our choice of the requisite pulse parameters is based on the consideration of the overall sensitivity of the pumping process to variation in some of these parameters.

The composition of the residual wave packet on the ground electronic level in terms of vibrational states, at the end of a 15 fs pulse, with three different peak intensities (I^0 = 1 $\times$ 10^{14}, 3.5 $\times$ 10^{14}, and 5 $\times$ 10^{14}, W/cm^2) have been shown for three different initial vibrational levels v = 0, 2, and 4 in Figs. 1(a)–1(c), respectively. After the pump pulse is over the evolution of this wave packet on the ground-state potential surface continues without change in its composition in terms of the vibrational eigenstates. It is evident from Fig. 1(a) that a laser field of peak intensity 1 $\times$ 10^{14} W/cm^2 has very little impact on the initial $v = 0$ stationary state. The dissociation is insignificant and the final wave packet almost retains its stationary character with only a small contribution from the $v = 1$ level. Laser fields of higher peak intensities, e.g., I^0 = (3.5 and 5) $\times$ 10^{14} W/cm^2 are also not effective in inducing molecular dissociation from the v = 0 level. However, such increased pump laser fields do lead to appreciable deformation of the field-induced potential compared to the field-free values. Motion of the initial wave packet in this distorted potential results in increased contribution of the excited vibrational states in the final nonstationary coherent wave packet. When the initial level is an excited vibrational level, as in Figs. 1(b) and 1(c), the residual wave packet contains vibrational components with both higher and lower vibrational quantum numbers. The proportion of higher vibrational levels increases with increase of peak intensity of the pump pulse. For the initial state v = 2, after the pump pulse with a peak intensity of 10^{14} W/cm^2, a measurement of the vibrational quantum number of the undissociated molecules will yield a distribution mostly between $v = 1$ and $v = 5$. As the intensity is increased, this distribution becomes broader. For a 15 fs pulse of peak intensity I_0 = 3.5 $\times$ 10^{14} W/cm^2, almost half of such measurements will yield values between v = 4 and 10. The distribution has a local maximum at v = 6. When the intensity is increased to 5 $\times$ 10^{14} W/cm^2, a bimodal distribution is obtained with maxima at $v = 3$ and $v = 10$ along with a significant contribution from v = 0. The nodes in the distribution occur at $v = 1$ and v = 5–6. A similar phenomenon

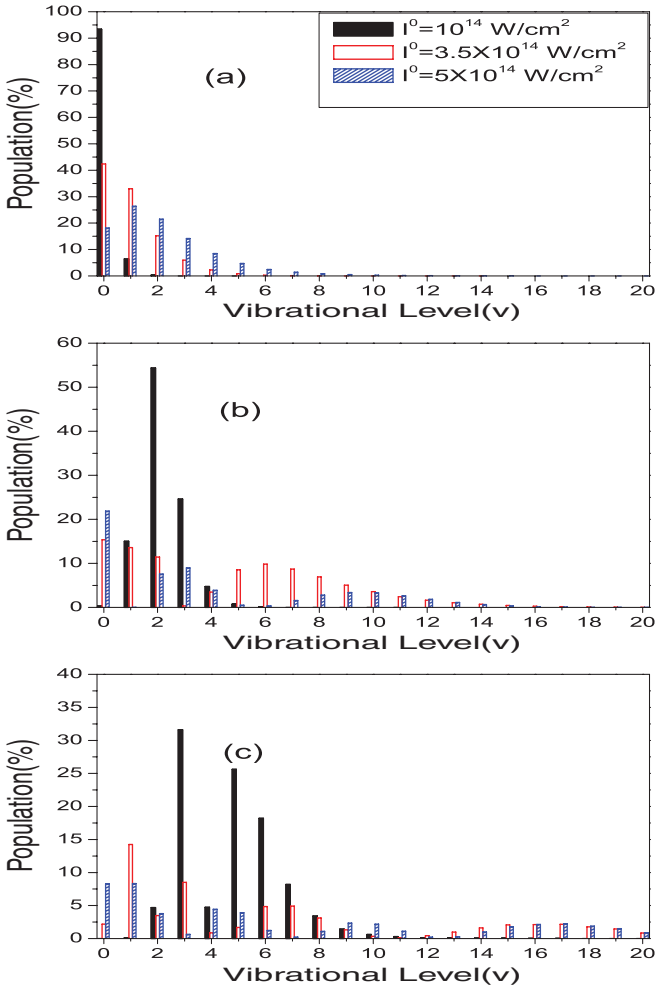

FIG. 1. (Color online) Vibrational distribution in the residual wave packets obtained at the end of a 15 fs, 1060 nm wavelength laser pulse of three different intensities for initial states: (a) $v = 0$, (b) $v = 2$, and (c) $v = 4$, respectively.

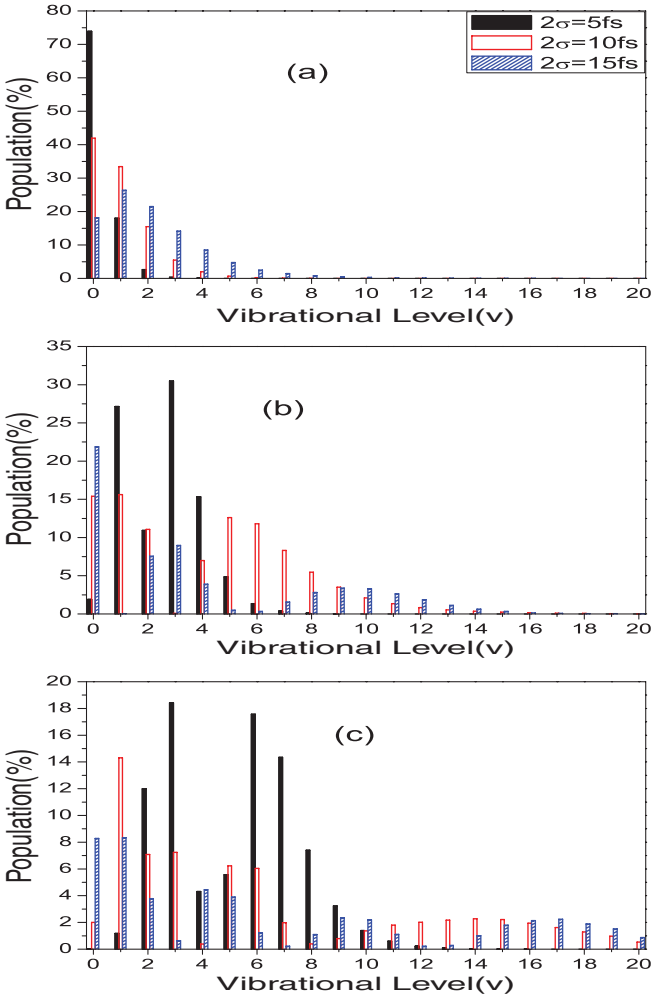

FIG. 2. (Color online) Vibrational distribution in the residual wave packets created by three different pulse times with the peak intensity, $I^0 = 5 \times 10^{14}$ W/cm^2 of a 1060 nm wavelength laser pulse for initial states: (a) $v = 0$, (b) $v = 2$, and (c) $v = 4$, respectively.

occurs for the initial state $v = 4$. At the lowest intensity vibrational excitation up to v = 8 or 9 will be observed, but at the higher intensities, the resulting residual wave packet will have significant components of highly excited states with $v = 14$–20.

As mentioned earlier, the outward motion of the initial wave packet on the potential surfaces distorted by the radiative couplings due to the pump pulse cause vibrational excitations. The greater the intensity of the pulse used, the greater will be the extent of the outward movement [38]. Also, the larger the duration of the pulse, the more time will the wave packet get for moving away from its initial equilibrium position. This will have two consequences. First, for higher intensities and/or larger pulse durations the residual wave packet will have a greater spatial spread resulting in a higher proportion of vibrationally excited states in the final wave packet. On the other hand, after the pulse a larger fraction of the wave packet will be found within the vibrational continuum. Thus the norm of the residual wave packet will be depleted through multiphoton dissociation. Again, for a given peak intensity and pulse time, both these effects will be higher for higher initial vibrational states. For a peak intensity $I^0 = 1 \times 10^{14}$ W/cm^2 of a 15 fs pulse the field-induced molecular dissociation is insignificant (for $v = 0$, 2, and 4). In the case of the $v = 2$ level the probability of dissociation is about 6% at $I^0 = 3.5 \times 10^{14}$ W/cm^2 and about 40% at $I^0 = 5 \times 10^{14}$ W/cm^2, respectively. For the initial level $v = 4$ the dissociation probability is about 40% and 50% for these two peak intensities. We have also found that field-induced transitions mediated by the permanent dipole moment, which may cause transfer of population between the vibrational levels of the ground electronic state, are not significant for the spatiotemporal evolution of the wave packet in our case and such processes do not affect the vibrational distribution due to the pump process.

Figure 2 demonstrates the role of pulse duration in the formation of coherent vibrational wave packets of HD^+. Here vibrational distributions in the residual wave packets are plotted for three different pulse times, and for the three different initial vibrational states chosen in our calculations, keeping the peak intensity of the laser field fixed at 5×10^{14} W/cm^2. Even the pulse with the 15 fs duration does not succeed in initiating the dissociation process from the ground

vibrational state $v = 0$ at this high intensity (the dissociation probability is only 0.05%). However, as demonstrated in Ref. [38], for such intense pulses, the avoided gap in the adiabatic potential arising from a seven-photon crossing may allow the wave function for $v = 0$ to move to larger values of the internuclear separation R before the peak intensity is reached, resulting in a significant presence of vibrationally excited states in the final wave packet. In the case of very short pulses the avoided crossings disappear before an appreciable portion of the wave packet is able to escape through the opening. As a result, for total pulse duration of 5 fs, the final wave packet shows only a slight deviation from its original, stationary form and is mainly confined to a small internuclear separation region. The result is a predominant contribution of the $v = 0$ level with a small mixture of the $v = 1$ state and an even smaller mixture of the $v = 2$ level in the wave packet. In the case of the spatially extended higher initial states the release of wave-packet components through the laser-induced avoided crossings is more favorable and therefore the wave packet can traverse regions of larger internuclear separations resulting in broader vibrational distribution displayed in Figs. 2(b) and 2(c).

From the results displayed in Figs. 1 and 2 it is evident that starting from $v = 0$, a unimodal vibrational distribution is obtained for all combinations of the pulse duration and peak intensity. The longest pulse investigated effected a change of the position of the mode in this distribution from $v = 0$ to $v = 1$ when the peak intensity was increased to 5×10^{14} W/cm^2 as seen from Figs. 1 and 2. However multimodal distributions are obtained from vibrationally excited initial states. In the case of $v = 4$, even at $I^0 = 1 \times 10^{14}$ W/cm^2, a multimodal distribution is observed in Fig. 1(c). The increase of the peak intensity as well as the pulse duration actually stretches the vibrational distribution of the residual population on the ground electronic state resulting in a shift of the mode positions both toward lower and higher vibrational quantum numbers away from the initial value of v. We also note the absence of specific v values in these multimodal distributions for particular combinations of pulse time and peak intensity. Thus for excited initial states, different types of localized coherent vibrational wave packets can be generated by changing the pulse parameters.

To examine the influence of temporal pulse shapes on the constitution of the wave packet we have compared our sin^2 pulse results with the vibrational distribution obtained using a Gaussian pulse with the same peak intensity and FWHM. The electric field intensity of the Gaussian pulse, unlike that in the sin^2 pulse, goes to zero only at infinite times. The results are shown in Fig. 3 for the initial state $v = 4$ and for different sets of pulse time and peak intensity. The discrepancy between the Gaussian and sin^2 results is much less for other initial states, i.e., $v = 0$ and $v = 2$ used in our calculations.

Earlier, in the context of ionization, it was argued that a pulse which vanishes only at infinite times would be more appropriate to reproduce experimental results by taking early pulse cycle ionization into account [42]. In the present case of molecular excitation and fragmentation we notice a somewhat lower dissociation yield (0.26) for a Gaussian pulse with a 5 fs FWHM compared to that obtained from the corresponding sin^2 pulse of total duration 10 fs (0.35). However, for a FWHM of 7.5 fs the yield is greater for the Gaussian pulse compared to the

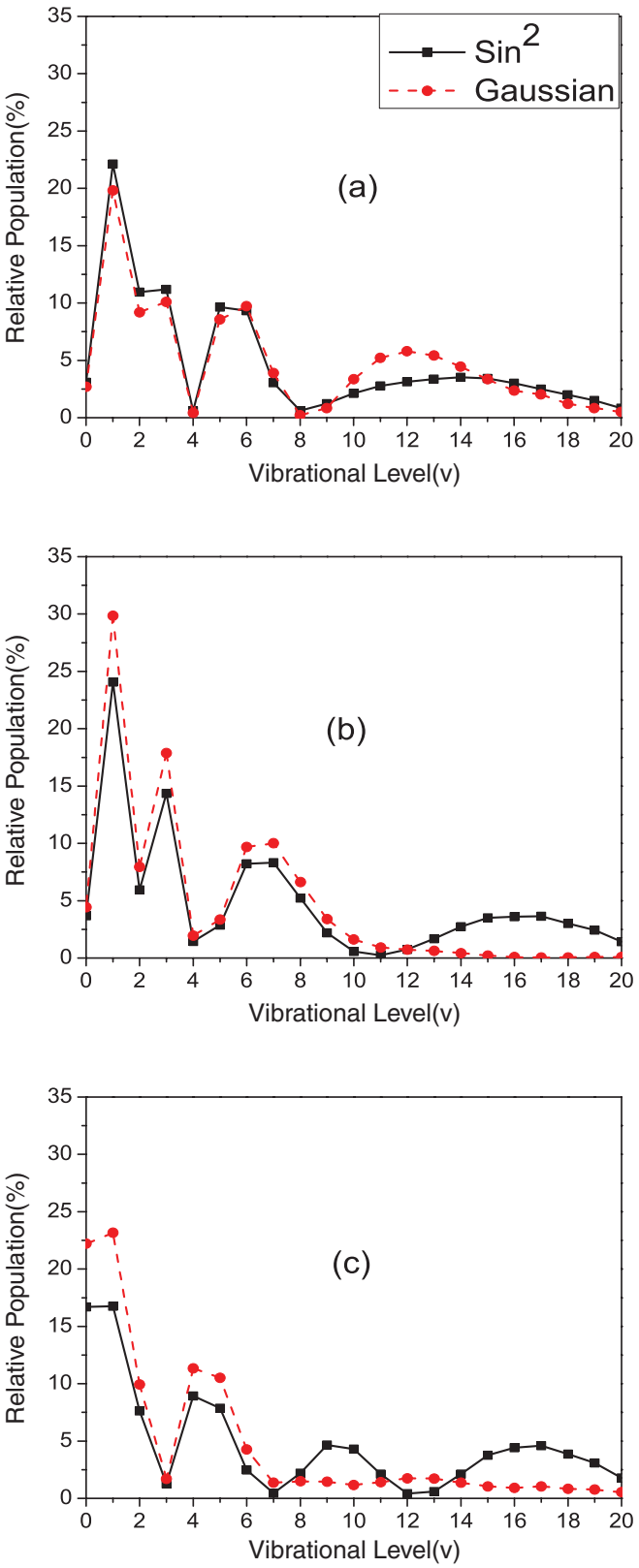

FIG. 3. (Color online) Relative population in the residual wave packet is plotted as a function of the vibrational quantum number using two different temporal pulse shapes, sin^2 and Gaussian, having the same peak intensity and FWHM starting from initial state $v = 4$ for (a) FWHM = 5 fs, $I^0 = 5 \times 10^{14}$ W/cm^2, (b) FWHM = 7.5 fs, $I^0 = 3.5 \times 10^{14}$ W/cm^2, and (c) FWHM = 7.5 fs, $I^0 = 5 \times 10^{14}$ W/cm^2.

$\sin^2$ pulse for both the peak intensities. The yields for the $\sin^2$ pulses are 0.4 and 0.5 for $I^0 = 3.5 \times 10^{14}$ and 5×10^{14} W/cm^2, respectively. The yields for the corresponding Gaussian pulses are 0.53 and 0.64, respectively. The relative proportion of the higher vibrational states generally decrease for a Gaussian pulse, though for the 5 FWHM Gaussian pulse a few excited vibrational state components have greater magnitudes than those obtained using the corresponding $\sin^2$ pulse.

Unlike the ionization case, the early pulse cycles do not appreciably affect the structure of the nuclear wave packet, presumably because of its larger mass compared to that of an electron. However, the part of the wave packet that has moved to a sufficiently large distance will be influenced by the weak residual part of the Gaussian pulse unlike the $\sin^2$ pulse which vanishes at twice the FWHM time. The presence of this weak residual field coupling helps some portion of the wave packet at very large distances to escape through the avoided crossings, provided sufficient time is left for allowing this passage. Thus for a 7.5 fs FWHM Gaussian pulse, the weak residual field couplings at large R keep the potentials open for a longer period of time and consequently, the higher energy parts of the wave packet are depleted through dissociation [Figs. 3(b) and 3(c)]. The picture for a 5 fs FWHM pulse is slightly different, because in this case the couplings become very weak much sooner and a considerable portion of the higher energy components of the wave packet remains trapped when the couplings are effectively turned off. This results in a slightly higher proportion of vibrational states with $v = 10$–14 for the Gaussian pulse [Fig. 3(a)]. Our following discussions will be based on the wave packet excited by the $\sin^2$ pulses only.

Figure 4 illustrates the evolution of the wave packet on the ground electronic potential of HD^+ for a 15 fs $\sin^2$ pulse of peak intensity 5×10^{14} W/cm^2, starting from an initial stationary state $v = 0$ in Fig. 4(a) and $v = 2$ in Fig. 4(b). It is seen how the field-induced distortion of the potential results in considerable spreading of the wave packet, so when at the end of the pulse the gap between the adiabatic potentials is closed, a portion of the wave packet remains in a region well away from the equilibrium internuclear separation with R greater than 3 a.u. giving rise to some vibrational excitation. It is also seen that no part of the wave packet escapes into the large R region, but its subsequent evolution gives indication of the considerable presence of excited vibrational state components. In Fig. 4(b) the initial wave function with $v = 2$ has a greater extension to start with, and the portion of the wave packet at large R moves faster through the gap due to higher kinetic energy as well as its proximity to the five-photon crossing region, resulting in a greater distortion of the wave packet. An appreciable portion of the wave packet is now present in a region beyond ~5 a.u. when the gap closes. This portion eventually moves toward the asymptotic region and would finally dissociate. The undissociated fraction is composed of highly excited vibrational levels. We get a much broader distribution of vibrational states in the residual wave packet with major contributions from the higher excited states with vibrational quantum numbers up to $v = 12$.

After the first pulse gets over, the vibrational composition of the residual coherent wave packet may be analyzed using a time-delayed weak probe pulse. This delay time (τ_2) must

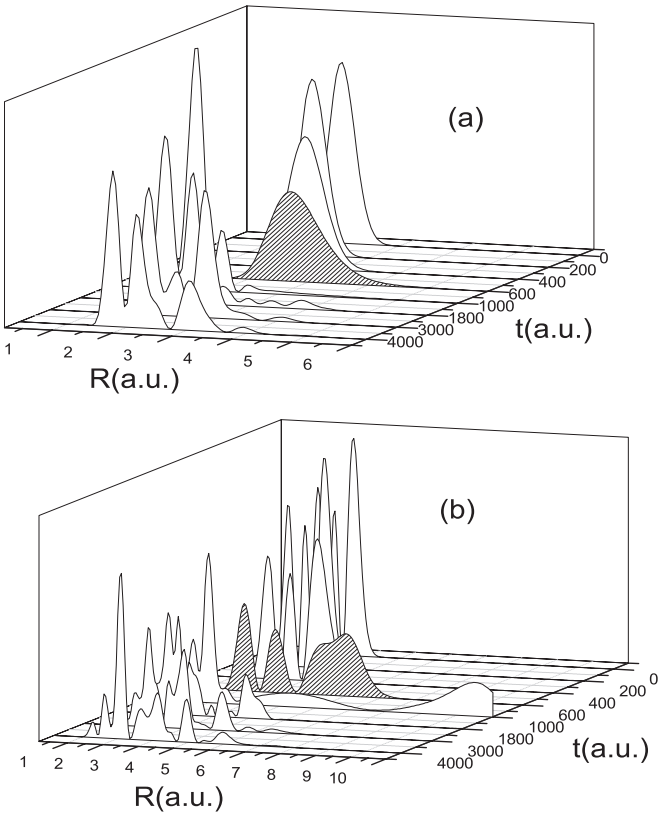

FIG. 4. Wave-packet evolution initiated by a 1060 nm wavelength laser pulse of duration 15 fs and intensity 5×10^{14} W/cm^2 for initial vibrational level (a) $v = 0$ and (b) $v = 2$. The shaded portion denotes the wave-packet shape near the end of the pulse.

be sufficiently large to allow wave-packet portion in the vibrational continuum to cross over into the asymptotic region and stop them from interfering with the dissociation signal caused by the second probe pulse. Any such component present in the interaction region during the application of the probe pulse will give a continuous background in the kinetic-energy spectra of the photofragments generated by the probe. The time delay (τ_2) is set at 8000 a.u. (~193 fs) because of our use of a large interaction region. However, once sufficient delay time is allowed, the interpulse delay as such does not play any significant role. This is primarily due to our use of a probe pulse of sufficiently large duration (4000 a.u. ~ 96 fs and 10000 a.u. ~ 240 fs), which allows scanning through all possible spatial structures of the coherent wave packet (which continues to change shape as shown in Fig. 4) to be probed. The large duration of the weak probe pulse is also important for inducing appreciable dissociation of the bound wave packet by photons of well-defined energy. The field strength is kept low in order to allow only single-photon bond dissociation. Thus the kinetic-energy distribution of the photofragments arising from single-photon dissociation by the probe pulse consists of well-resolved peaks which can be correlated to the different vibrational states present in the coherent wave packet.

We have used dissociating pulses of two different durations, 96 and 240 fs, respectively, with comparatively low peak intensities of $(1,5,10) \times 10^{11}$ W/cm^2 as probes of the residual vibrational wave packet on the ground electronic state. The

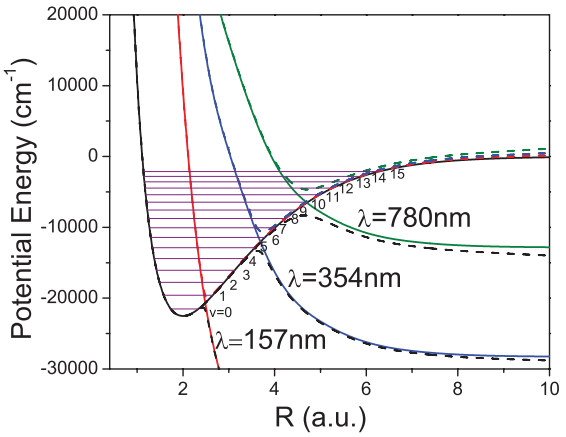

FIG. 5. (Color online) Single-photon dressed potential energy curves and the corresponding adiabatic potentials at $I^0 = 5 \times 10^{11}$ W/cm^2 for three different probe wavelengths 157, 354, and 780 nm, respectively. The solid lines represent the dressed potentials and the dashed lines represent the corresponding adiabatic potentials.

kinetic-energy distribution of the photofragments generated by this probe pulse acting on the nonstationary wave packet created by the first pulse is obtained by propagation of the wave-packet components until the end of the probe pulse and analyzing its momentum space representation in the asymptotic region. The most obvious feature of the photodissociation during wave-packet probing is that the different vibrational components are affected to different extents by the probe pulse. We have taken three different wavelengths of the probe pulse: 157, 354, and 780 nm. The observation of the single-photon kinetic-energy spectrum constitutes a measurement which should indicate a specific vibrational state of the molecule before dissociation. In Ref. [34] an attempt was made to relate the kinetic-energy spectra obtained after predissociation along a repulsive potential of the H_2 molecule with the vibrational levels of H_2^+, obtained by the electron impact ionization of the H_2 molecule. It was shown that the area under each peak, corresponding to a different kinetic energy is proportional to the population of the specific vibrational level. In our case, for investigation of the molecules in three different regions of vibrational excitation, we use three different wavelengths of the probe pulse. Figure 5 gives a simplified representation of the diabatic as well as the field-modified adiabatic potential surfaces for these three wavelengths, taking into account only the single-photon coupling between the ground and the excited electronic states. This figure has been drawn for a probe pulse of intensity $I^0 = 5 \times 10^{11}$ W/cm^2. The unperturbed vibrational level energies up to $v = 15$ are also shown.

It is seen from Fig. 5 that bond softening in the region of vibrational states 0–2 takes place only if the wavelength of 157 nm is used. Vibrational states 5–7 and 8–12 can be bond softened using radiation of wavelengths 354 and 780 nm, respectively.

Figure 6 shows the kinetic-energy distribution of the photofragments, arising from the dissociation of the coherent wave packet generated by a 15 fs pulse with a peak intensity 5×10^{14} W/cm^2, starting from an initial stationary state with $v = 2$. This wave packet is subjected to weak ($I^0 = 5 \times 10^{11}$ W/cm^2) sine-squared probe pulses of wavelengths 157, 354, and 780 nm. The results for 96 fs probe pulses are displayed in Figs. 6(a)–6(c) and those for 240 fs pulses have been shown in Figs. 6(d)–6(f). These are actually plots of the squared magnitudes of the momentum space wave-packet components in the asymptotic region, plotted against the kinetic energy of the photofragments. The values of kinetic energy at the peaks agree perfectly with those expected from single-photon dissociation from the field-free vibrational states. Thus the peaks can be interpreted as being due to dissociation of the vibrational levels present in the wave packet probably along the pathway defined by GS $\rightarrow$ ES $- 1\omega$. However, comparable peaks at the same energies are also seen due to one-photon dissociation on the ground potential surface GS. We have found that the existence of fragments corresponding to the asymptotic state of the GS potential must be explained as being due to nonadiabatic transitions [39]. It would also be of interest to investigate whether the height of the different peaks in the kinetic-energy release spectra can be related to the proportion of the corresponding vibrational levels in the concerned wave packet.

We first note that some of the prominent peaks in the kinetic-energy spectra of the 96 fs probe pulse are either missing or relatively weakened in the kinetic energy spectra obtained by probing with the 240 fs pulse. For example, in Fig. 6(a) we find a peak of appreciable magnitude corresponding to the $v = 2$ level. But this peak almost disappears from the spectrum when we increase the duration of the probe pulse to 240 fs, as evident from Fig. 6(d). An increase in the duration of the probe pulse from 96 fs to 240 fs results in an increase in the absolute value of the dissociation probability from 0.04 to 0.09. Therefore in keeping with the increase in the dissociation probability as the pulse time increases, a proportionate increase in the absolute value of the kinetic-energy peak height corresponding to each particular vibrational quantum number was expected. However, we observe from Figs. 6(a) and 6(d), an enhancement in the magnitude of the peak height corresponding to the $v = 0$ level by a factor of 5 along with dips in the peak height for the $v = 2$ level and a relative decrease of the height of the peak corresponding to $v = 3$ with respect to that for $v = 0$. Pulse time variation of the probe pulse actually influences the dynamics of the nuclear wave packet, changing its constitution in different ways and thereby affecting the relative peak heights in the kinetic-energy spectra. We also observe the notable absence of energy peaks arising from the $v = 4$ level during probing by a 157 nm laser pulse in both Figs. 6(a) and 6(d), in spite of appreciable contribution of these levels in the overall vibrational composition as shown in Fig. 1.

Figures 6(b) and 6(e) display the kinetic-energy release spectra due to dissociation induced by a 354 nm laser field, acting on the coherent vibrational wave packet prepared from the $v = 2$ level of the ground electronic state, for these two pulse times. In each of the two cases we obtain corresponding peak positions in the kinetic-energy release spectra for almost all the vibrational levels that are possibly affected by the 354 nm probe pulse. However, an interesting anomaly can be observed while we compare the peak heights of the different kinetic-energy peaks to that with the initial population of the vibrational levels. For the four neighboring vibrational levels $v = 7$, 8, 9, and 10, the $v = 7$ level has the lowest while $v = 9$ and $v = 10$ have the highest contribution in the

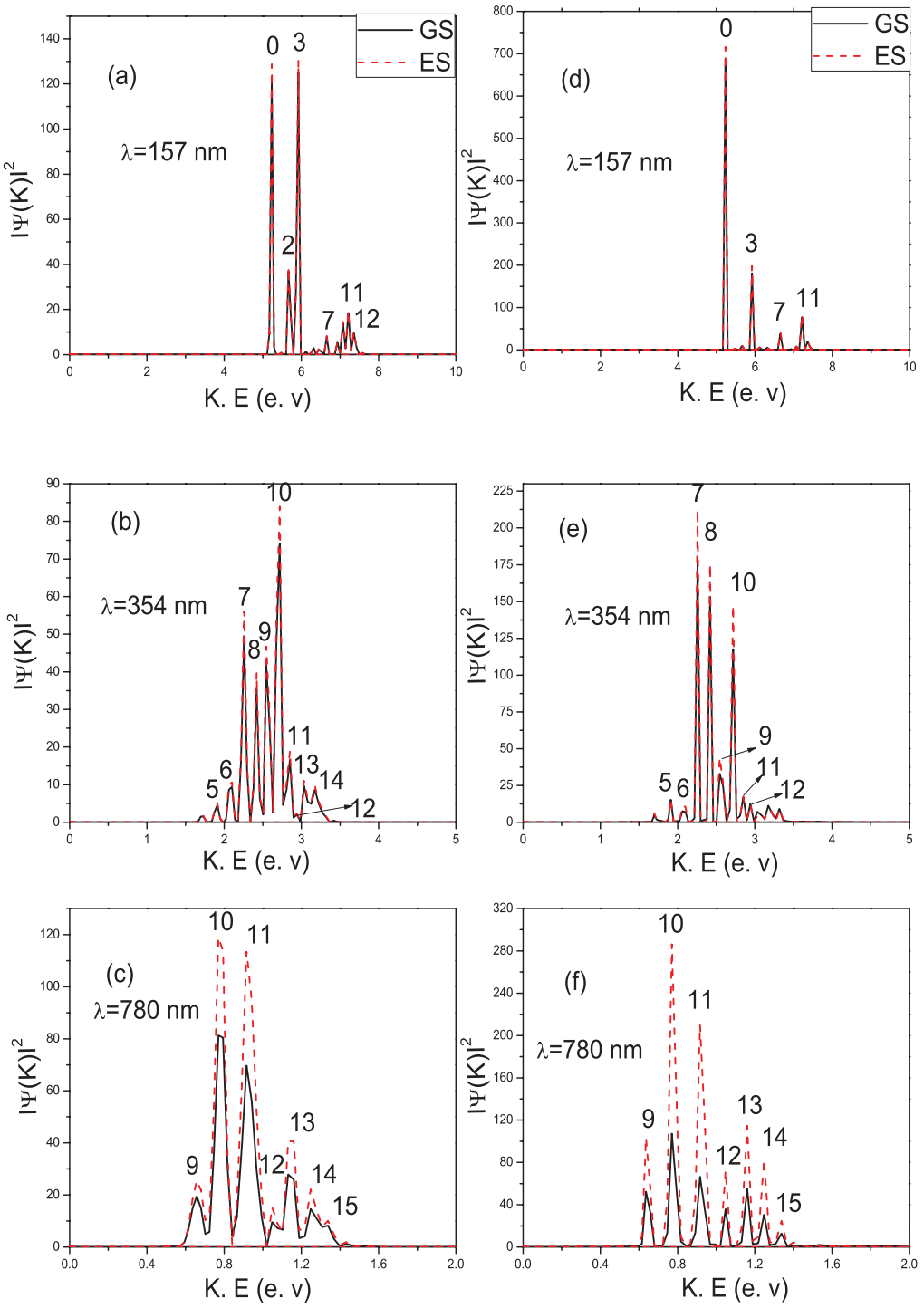

FIG. 6. (Color online) Kinetic-energy spectra of the photofragments obtained from the wave packet created by a 1060 nm, 15 fs pulse of peak intensity 5×10^{14} W/cm^2 from an initial state $v = 2$, for the probe pulse of $I^0 = 5 \times 10^{11}$ W/cm^2 and duration 96 fs in the case of (a), (b), and (c) and 240 fs in the case of (d), (e), and (f) for the respective probe wavelengths.

wave packet being probed. However, marked differences in the pattern of peak heights for these four adjacent vibrational levels in the kinetic-energy spectra can be observed for the two different durations of the probe pulse. In Figs. 6(b) and 6(e) we observe that in spite of the lowest population of the $v = 7$ level in comparison to the $v = 8$, 9, and 10 levels in the wave packet being probed, the peak in the kinetic-energy spectrum corresponding to this level has the second highest magnitude for the 96 fs pulse and the highest for the 240 fs pulse. Again, in spite of comparable initial populations of the $v = 9$ and $v = 10$ levels, the peak height corresponding to the $v = 9$ level is lower than that from the $v = 10$ level for both the pulse times [Figs. 6(b) and 6(e)]. The relative heights of the peaks are also significantly altered when we change the probe

time. For the longer, 240 fs pulse, unlike that of the 96 fs pulse, the peak height in the kinetic-energy release (KER) spectra corresponding to the $v = 9$ level is very much less in magnitude compared to that corresponding to the $v = 8$ level, even though initial population of the $v = 9$ level is greater compared to that of the $v = 8$ level.

In the case of probing by 780 nm pulse for both the cases shown in Figs. 6(c) and 6(f) vibrational levels lower than the $v = 9$ level remain trapped inside the lower adiabatic potential well, thereby accounting for their absences in the kinetic-energy distribution. It is evident from our results that well-resolved peaks are obtained for nearly all the excited vibrational levels present in the wave packets being probed. However, like in the previous case, here we also find a similar instance of the reversal of peak heights corresponding to $v = 12$ and $v = 13$ levels with respect to the magnitudes of the coefficients of these levels in the initial wave packet. This is true for both the pulse times.

Earlier in Ref. [43] it has been argued that the variation in relative heights of the peaks corresponding to different vibrational levels in photofragment kinetic-energy spectrum can be simply explained by perturbation theory without invoking dynamical effects like population trapping, etc. In this explanation any observed discrepancy between the wave-packet composition and the kinetic-energy peak sizes should arise only due to suppressed dipole coupling effects, which is the decrease in the magnitude of the bound-continuum dipole matrix elements for certain values of v when the exciting wavelength is kept constant. In Ref. [44] it was shown according to perturbation theory that for relatively weak laser fields the peak heights in the kinetic-energy distribution are proportional to the product of the initial population of the bound state and the corresponding Franck-Condon factor. From our results it appears that the change in relative heights of the peaks with pulse duration in some cases indicates that the dynamical evolution of the wave packet plays a role, especially in the case of probing by a long pulse. We use the perturbation calculations for our weak-field case for making a qualitative comparison with the full molecular dynamical calculations.

In Fig. 7 we plot the relative heights of the kinetic-energy peaks corresponding to various vibrational states for two different durations of the probe pulse (96 and 240 fs), along with the relative heights expected from perturbation theory calculations as functions of the vibrational quantum number v for the three-probe laser wavelengths used. The perturbation results are obtained by multiplying the squares of the relevant bound-continuum matrix elements of the transition dipole moment with the squared coefficient of the particular vibrational level in the wave packet. The time-dependent wave-packet calculations have been performed for a peak intensity of 5×10^{11} W/cm^2 and the computed results for the three probe wavelengths have been shown separately. The normalization in the three cases has been made with respect to the magnitudes of the peak heights corresponding to $v = 0$, 7, and 10, respectively.

For nearly all the cases in Fig. 7 the expected relative pattern of the peaks obtained from perturbation theory is in good qualitative agreement with the full time-dependent calculations. In particular, suppressed dissociation of specific vibrational states appears to be in conformity with the reduced

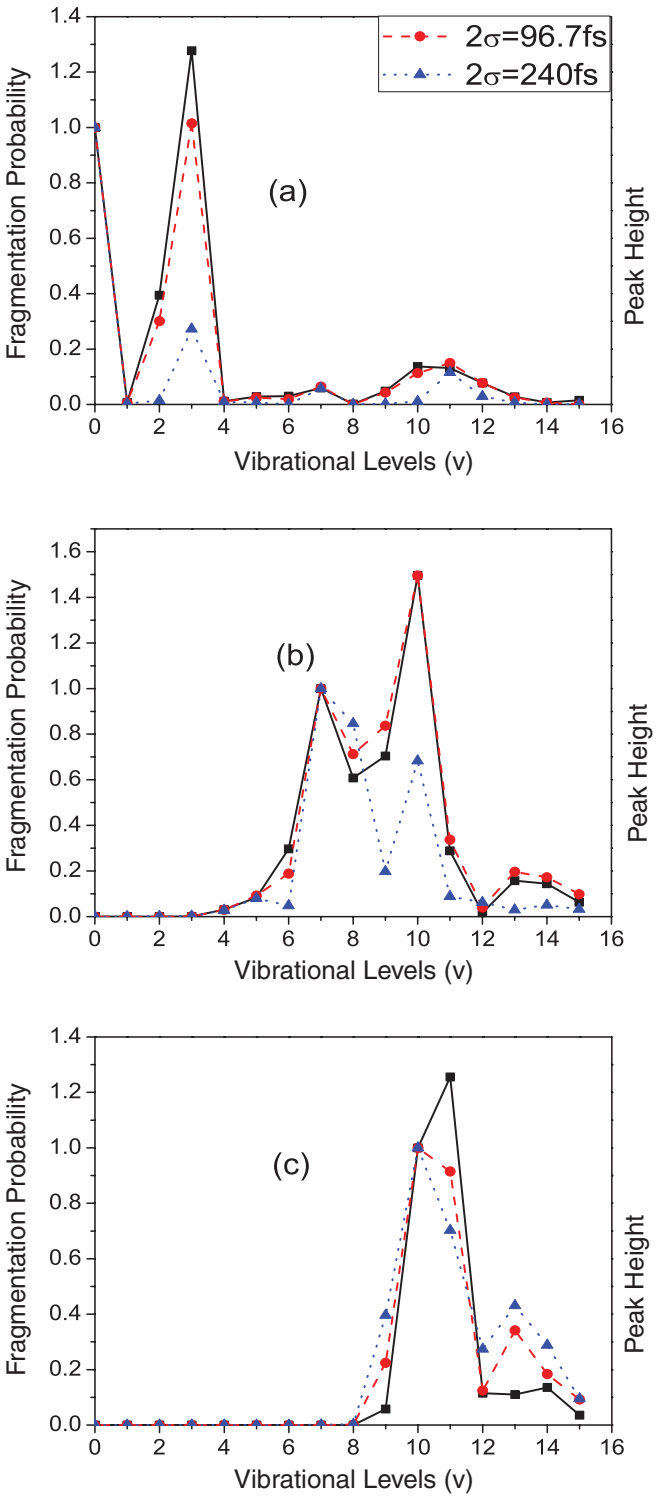

FIG. 7. (Color online) Normalized results of photofragmentation probability of the different vibrational eigenstates in the wave packet, created by a 1060 nm, 15 fs pulse of peak intensity 5×10^{14} W/cm^2 from an initial state $v = 2$, calculated from perturbation theory. The magnitudes of the peak heights in the kinetic-energy spectra are also plotted as functions of vibrational quantum number for $2\sigma = 96$ fs and 240 fs and $I^0 = 5 \times 10^{11}$ W/cm^2 for wavelengths (a) 157, (b) 354, and (c) 780 nm, respectively. The solid lines represent the fragmentation probability and the dashed and dotted lines represent the kinetic-energy peak heights.

dipole coupled transition probabilities obtained from the perturbation calculations [43]. For instance, in the KE spectrum for 780 nm laser wavelength, the dip in the dissociation of the $v = 12$ state compared to its neighboring vibrational levels can be surely accounted for by a corresponding reduction in the bound-continuum dipole coupling matrix element for this particular vibrational state. Similarly the absences of the peaks corresponding to dissociation from the $v = 4$ state in the KER spectra for 157 nm may be attributed to the vanishing of the dipole matrix element as seen in Fig. 7(a). We can also say that there is also a nice quantitative agreement with the perturbation theory results for the shorter probe pulse. However for the 240 fs pulse, some discrepancies remain. For example, for the 157 nm, 240 fs pulse the suppressed dipole coupling effect alone is not sufficient for explaining the quantitative discrepancies between the normalized perturbation results and the full time-dependent calculations for peak heights corresponding to the $v = 2$ and $v = 3$ levels. Similar discrepancies are observed also for the larger wavelengths. In Fig. 7(b) the pattern of variation of the perturbation results simply reproduces the pattern displayed in Fig. 6(b) for the 96 fs pulse. But the decreased peak height of the $v = 10$ level in comparison to the $v = 7$ level for the long pulse is not in conformity with the predictions from the perturbation theory. More interestingly, for the 354 nm, 240 fs pulse, the decrease in the photofragments corresponding to dissociation from the $v = 9$ level, compared to that of $v = 8$, cannot be explained simply on the basis of suppressed dipole coupling effects. In fact a shift from the $v = 8$ level to the $v = 9$ level in Fig. 7(b), according to perturbation theory should result in increased dissociation. This actually happens for the 96 fs pulse, but for the 240 fs pulse a suppression of the corresponding peak in the kinetic-energy release spectra is observed. We note that for the low intensities of the probe pulse the field-free eigenenergy of the $v = 9$ level closely matches that of the $v = 1$ bound level in the upper adiabatic potential. (Energy difference is of the order of 10^{-5} a.u. for $I^0 = 1 \times 10^{11}$ W/cm^2 and 10^{-3} a.u. for $I^0 = 5 \times 10^{11}$ W/cm^2). This eventually may lead to laser-induced population trapping with corresponding quenching of the dissociation rate from this particular level due to resonance stabilization at a diabatic-adiabatic energy coincidence [45]. Thus it appears that for the longer pulse there is sufficient time for the setting up of additional dynamical pathways that can influence the overall probing process. Detailed investigation of the wave-packet dynamics involved especially for cases relating to large pulse times is continuing.

Thus from the above discussion inferences can be drawn that for probing the composition of coherent vibrational wave-packets pulses of moderate durations are more favorable.

In order to study the intensity effects of the probe pulse on the overall molecular dynamics during the probing we perform the calculations at three different peak intensities $I^0 = (1, 5,$ and $10) \times 10^{11}$ W/cm^2 for $2\sigma = 96$ fs for all three-probe frequencies. The results are shown in Fig. 8. As such no additional discrepancies in the pattern of variation of the peak heights from the perturbation results arises due to variation of peak intensity. Although the best matching between the results from the two sets of calculations is attained at the lowest peak intensity, it would be fair to conclude that within the range

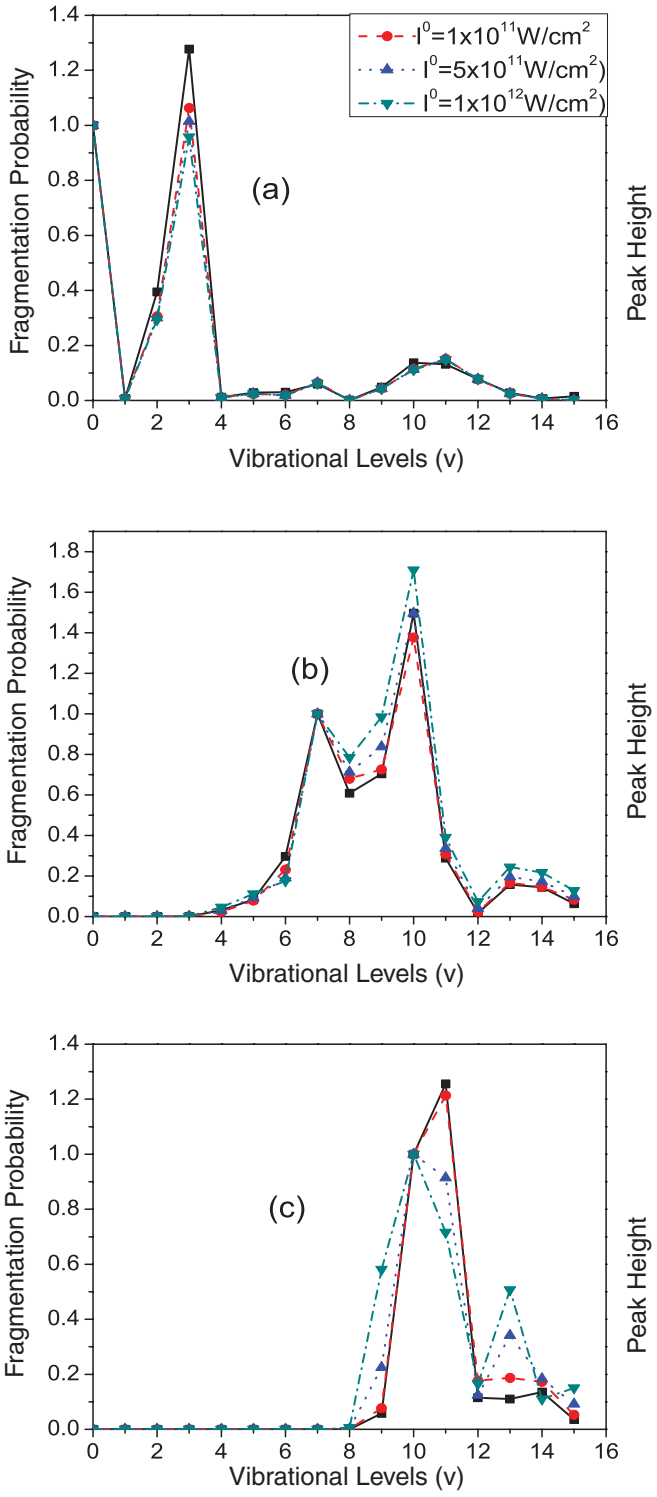

FIG. 8. (Color online) Normalized results of photofragmentation probability of the different vibrational eigenstates in the wave packet, created by a 1060 nm, 15 fs pulse of peak intensity 5×10^{14} W/cm^2 from an initial state $v = 2$, from perturbation theory. The magnitudes of the peak heights in the kinetic-energy spectra are also plotted as functions of vibrational quantum number for $2\sigma = 96$ fs and $I^0 = 1 \times 10^{11}$ W/cm^2, 5×10^{11} W/cm^2, and 1×10^{12} W/cm^2 for wavelengths (a) 157, (b) 354, and (c) 780 nm, respectively. The solid lines represent the fragmentation probability and the dashed, dotted, and dash-dotted lines represent the kinetic-energy peak heights.

of intensities studied, the field strength of the probe pulse does not have any significant influence in the overall probing process.

IV. CONCLUSION

We have explored the formation of coherent wave packets on the ground electronic state of a HD^+ molecular ion from different stationary eigenstates through impulsive excitation by an intense ultrashort laser field. Both $\sin^2$ and Gaussian pulse shapes have been used. For each initial state the variation of the pump pulse parameters, namely, the duration and peak intensity of the laser field, can be used to change the composition of the coherent vibrational wave packet by controlling its spatial and temporal evolution. We have also investigated the possibility of determination of this composition by exposing the resulting wave packet to a weak and comparatively long delayed probe pulse of a particular frequency. This frequency is determined by the vibrational quantum numbers in whose presence we are interested. The delay between the two pulses as well as the temporal length of the probe pulse should be sufficiently large for obtaining well-defined kinetic-energy peaks which can be correlated to energies of single-photon dissociation fragments arising from specific vibrational levels constituting the wave packet. The comparison of our numerical results for the kinetic-energy spectra with those expected from perturbation theory calculations reveals the onset of different dynamical processes during the relatively long probing process which leads to certain discrepancies between the wave-packet composition and kinetic-energy peak sizes.

ACKNOWLEDGMENTS

One of the authors (S.C.) thanks the CSIR, New Delhi (Government of India) for the financial support for this work.

[1] A. Mokhtari, P. Cong, J. L. Herek, and A. H. Zewail, Nature (London) **348**, 225 (1990).
[2] L. R. Khundkar and A. H. Zewail, Ann. Rev. Phys. Chem. **41**, 15 (1990).
[3] H. Stapelfeldt, E. Constant, and P. B. Corkum, Phys. Rev. Lett. **74**, 3780 (1995).
[4] S. Chelkowski, P. B. Corkum, and A. D. Bandrauk, Phys. Rev. Lett. **82**, 3416 (1999).
[5] A. D. Bandrauk and S. Chelkowski, Chem. Phys. Lett. **336**, 518 (2001).
[6] A. D. Bandrauk and S. Chelkowski, Phys. Rev. Lett. **87**, 273004 (2001).
[7] B. Feuerstein and U. Thumm, Phys. Rev. A **67**, 063408 (2003); U. Thumm, T. Niederhausen, and B. Feuerstein, *ibid.* **77**, 063401 (2008).
[8] A. S. Alnaser *et al.*, Phys. Rev. A **72**, 030702(R) (2005).
[9] F. Légaré, K. F. Lee, I. V. Litvinyuk, P. W. Dooley, A. D. Bandrauk, D. M. Villeneuve, and P. B. Corkum, Phys. Rev. A **72**, 052717 (2005).
[10] Th. Ergler, A. Rudenko, B. Feuerstein, K. Zrost, C. D. Schröter, R. Moshammer, and J. Ullrich, Phys. Rev. Lett. **95**, 093001 (2005).
[11] Th. Ergler, A. Rudenko, B. Feuerstein, K. Zrost, C. D. Schröter, R. Moshammer, and J. Ullrich, Phys. Rev. Lett. **97**, 193001 (2006).
[12] Th. Ergler, A. Rudenko, B. Feuerstein, K. Zrost, C. D. Schröter, R. Moshammer, and J. Ullrich, J. Phys. B **39**, S493 (2006).
[13] B. Feuerstein, Th. Ergler, A. Rudenko, K. Zrost, C. D. Schröter, R. Moshammer, J. Ullrich, T. Niederhausen, and U. Thumm, Phys. Rev. Lett. **99**, 153002 (2007).
[14] A. Rudenko, Th. Ergler, B. Feuerstein, K. Zrost, C. D. Schröter, R. Moshammer, and J. Ullrich, J. Phys.: Conf. Series **88**, 012050 (2007).
[15] C. R. Calvert *et al.*, CLF Annual Report 2005-2006.
[16] J. Mckenna *et al.*, J. Phys: Conf. Series **58**, 375 (2007); C. R. Calvert *et al.*, *ibid.* **58**, 379 (2007).
[17] C. R. Calvert, W. A. Bryan, W. R. Newell, and I. D. Williams, Phys. Rep. **491**, 1 (2010).
[18] A. González-Castrillo, J. F. Pérez-Torres, A. Palacios, and F. Martin, Theor. Chem. Acc. **128**, 735 (2011).
[19] J. Mckenna *et al.*, J. Mod. Opt. **54**, 1127 (2007).
[20] W. A. Bryan *et al.*, Phys. Rev. A **76**, 053402 (2007).
[21] C. R. Calvert *et al.*, J. Mod. Opt. **56**, 1060 (2009).
[22] E. Skovsen, M. Machholm, T. Ejdrup, J. Thøgersen, and H. Stapelfeldt, Phys. Rev. Lett. **89**, 133004 (2002).
[23] D. Brinks, F. D. Stefani, F. Kulzer, R. Hildner, T. H. Taminiau, Y. Avlasevich, K. Müllen, and N. F. van Hulst, Nature (London) **465**, 905 (2010).
[24] H. Katsuki, H. Chiba, B. Girard, C. Meier, and K. Ohmori, Science **311**, 1589 (2006).
[25] E. Goll, G. Wunner, and A. Saenz, Phys. Rev. Lett. **97**, 103003 (2006).
[26] Th. Ergler, B. Feuerstein, A. Rudenko, K. Zrost, C. D. Schröter, R. Moshammer, and J. Ullrich, Phys. Rev. Lett. **97**, 103004 (2006).
[27] I. V. Hertel and W. Radloff, Rep. Prog. Phys. **69**, 1897 (2006).
[28] C Altucci, R. Velotta, and J. P. Marangos, J. Mod. Opt. **57**, 916 (2010).
[29] H. Niikura and P. B. Corkum, Adv. At., Mol., Opt. Phys. **54**, 511 (2007).
[30] M. Lein, Phys. Rev. Lett. **94**, 053004 (2005).
[31] S. Baker, J. S. Robinson, C. A. Haworth, H. Teng, R. A. Smith, C. C. Chirila, M. Lein, J. W. G. Tisch, and J. P. Marangos, Science **312**, 424 (2006).
[32] S. Haessler, J. Caillat, and P. Salières, J. Phys. B **44**, 203001 (2011).
[33] H. Niikura, F. Légaré, R. Hasbani, A. D. Bandrauk, Misha Yu. Ivanov, D. M. Villeneuve, and P. B. Corkum, Nature (London) **417**, 917 (2002); H. Niikura, F. Légaré, R. Hasbani, M. Yu. Ivanov, D. M. Villeneuve, and P. B. Corkum, *ibid.* **421**, 826 (2003).
[34] X. Urbain, B. Fabre, E. M. Staicu-Casagrande, N. de Ruette, V. M. Andrianarijaona, J. Jureta, J. H. Posthumus, A. Saenz, E. Baldit, and C. Cornaggia, Phys. Rev. Lett. **92**, 163004 (2004).

[35] M. Zohrabi, J. McKenna, B. Gaire, N. G. Johnson, K. D. Carnes, S. De, I. A. Bocharova, M. Magrakvelidze, D. Ray, I. V. Litvinyuk, C. L. Cocke, and I. Ben-Itzhak, Phys. Rev. A **83**, 053405 (2011).
[36] F. He and U. Thumm, Phys. Rev. A **81**, 053413 (2010).
[37] E. Charron, A. Giusti-Suzor, and F. H. Mies, J. Chem. Phys. **103**, 7359 (1995).
[38] R. Bhattacharya and S. S. Bhattacharyya, Phys. Rev. A **79**, 043415 (2009).
[39] S. Chatterjee, B. Dutta, and S. S. Bhattacharyya, Phys. Rev. A **83**, 063413 (2011).
[40] A. Carrington and R. A. Kennedy, Mol. Phys. **56**, 935 (1985).
[41] R. E. Moss and I. A. Sadler, Mol. Phys. **61**, 905 (1987).
[42] C. Altucci, V. Tosa, R. Velotta, and C. H. Nam, Phys. Rev. A **70**, 065402 (2004).
[43] J. McKenna, F. Anis, B. Gaire, N. G. Johnson, M. Zohrabi, K. D. Carnes, B. D. Esry, and I. Ben-Itzhak, Phys. Rev. Lett. **103**, 103006 (2009).
[44] A. Kondorskiy and H. Nakamura, Phys. Rev. A **66**, 053412 (2002).
[45] C. Lefebvre, T. T. Nguyen-Dang, and O. Atabek, Phys. Rev. A **75**, 023404 (2007).